Three-dimensional mapping of evolving internal waves during the Shallow Water 2006 experiment

Mohsen Badiey, Lin Wan and Aijun Song

Three-dimensional mapping of evolving internal waves during the Shallow Water 2006 experiment

Mohsen Badiey,[a] Lin Wan, and Aijun Song
College of Earth, Ocean and Environment, University of Delaware, Newark,
Delaware 19716
badiey@udel.edu, wan@udel.edu, ajsong@udel.edu

Abstract: Detailed knowledge of sound speed profiles and the sound speed profile's spatial and temporal variability resulting from internal waves (IWs) are indispensable to investigating significant acoustic field fluctuations in shallow water. A strategy to obtain a time-varying, three-dimensional (3D) IW temperature field is presented. It uses two types of simultaneous measurements: dense observations from a farm of thermistor strings and IW surface expressions from a ship-based radar. Using data from the Shallow Water 2006 experiment, the temperature field, over multiple kilometers in range, was reconstructed and, fed to a 3D acoustic model to demonstrate IW impacts on acoustic propagation.
© 2013 Acoustical Society of America

1. Introduction

Solitary internal waves are a common oceanic process on the continental shelf, where strong tides and stratification occur over irregular topography. It is well recognized in the acoustics community that accurate and adequate sampling of the ocean environment is critical to predictions of the acoustic fluctuations. This is especially true for studies of acoustic interactions with IWs in shallow water regions.[1] The reasons are two-fold: (1) Complicated interactions between acoustics and IWs and (2) the complexity and nonlinearity of the IW generation and propagation mechanisms. However, it is costly, or even cost-prohibitive, to obtain environmental input parameters with an adequate spatial resolution for use in acoustics models.

Early studies showed drastic large intensity fluctuations resulting from acoustic propagation through the IW field.[2] Such intensity fluctuations later were shown through experimental observation and theoretical studies to have a strong dependence on the angle between the acoustic track and the IW propagation direction.[3–5] The IWs can also horizontally refract (or reflect) sound, which is known as the horizontal Lloyd's mirror effect[6–8] in the waveguide. In all these studies, non-curved IW fronts were often assumed to obtain the physical understanding. Recently, the curvature of IWs was shown to be critical in modeling acoustic ducting effects.[9,10]

Understanding the acoustic variability due to the IW field requires detailed knowledge of the spatial and temporal evolution of the sound speed field induced by IWs. However, detailed mapping of the IWs remains a challenging research topic, due to the spatial dimensions and nonlinear dynamics of internal waves. Motions of the water particles induced by the IWs generate a variable horizontal surface current. The variable surface current interacts with the surface waves and modulates the sea surface roughness, which is visible on radar images of the sea surface.[11] Satellite optical sensors and synthetic aperture radars are widely used to provide synoptic images of the IWs in the oceans. While satellite and airborne remote sensing techniques can generate important parameters, such as the wave propagation direction, the number of solitons

---

[a]Author to whom correspondence should be addressed.

per wave packet, etc., these observations cannot provide information on the temporal evolution of the IW packets since they are severely under-sampled in time. Recently, ship-based X-Band radars have been used to extract time evolving surface signature of IWs.[12] However, these do not have information in the depth dimension. Here we present a combination of two strategies for mapping a propagating IW packet in shallow water, based on the Shallow Water 2006 (SW06) experiment. Among the many types of measurements available, we focus on utilizing two components of the SW06 database: temperature records from a densely sampled thermistor farm and radar images of the propagating IWs. This letter is organized as follows. Section 2 describes the IW observations during SW06. Section 3 shows a detailed reconstruction of the 3D temperature field using the simultaneously measured temperature data within the thermistor farm and ship radar images. The impact of the reconstructed IW field on 3D acoustic propagation is also presented. Section 4 presents the discussions and summary.

2. Internal wave observations during SW06 experiment

The SW06 experiment was a large-scale, multi-institutional experiment conducted on the New Jersey continental shelf.[13] During the experiment, a large number of thermistor strings were densely deployed in a compact area. These temperature sensors sampled the individual mooring locations for depth structure over an extended period of time (over 1 month). In addition, ship-borne X-Band radars were used to track the propagation of the IWs. A limited number of satellite images were also obtained during the experiment.

A satellite image taken on 13 August 2006 shows the spatial variation of the IW field as a snapshot [see Fig. 1(a)]. These IWs initiated at the shelf break and propagated toward the shore. Depending on parameters such as the region's bathymetry, the stratification of water column at the origin, and the strength of tidal forcing, they generally formed as an organized packet, which then could be refracted and/or diffracted. Two or more wave packets could interfere with each other and form complicated wave structures. Such phenomena can cause highly anisotropic sound speed profiles. The IW fronts inside circles (I), (II), and (III) in Fig. 1(a) show some of these pronounced features (e.g., interference and bifurcation of different IW wave fronts). Although the satellite image can provide synoptic information over a large area, it is usually available for only one snap shot per day. By contrast, *in situ* measurements of multiple thermistor strings can provide detailed temperature profiles over time sampled at half-minute intervals. Here, 18 thermistor arrays, referred to as the "thermistor farm" in this letter, were densely deployed within a 4 km × 4 km region. Figure 1(b) shows the locations of the thermistors. Most of the thermistor arrays, 15 out of 18, covered the water column between 14 and 40 m from the surface, while the other three (#54, #30, and #31) covered from 14 m to the sea bottom. These sensors recorded temperature profiles every 30 s over a 1-month period. The temperature data at each thermistor were linearly interpolated to a time grid of 2 s and a vertical spatial grid of 0.5 m. Figure 1(c) and 1(d) show IW measurements between 14 and 40 m from two thermistor arrays at mooring locations #15 and #5, respectively. It is noticed that as the IWs traveled from thermistor #15 at the south, toward the upper corner (thermistor #5), the solitons within the packet separated from each other and changed from an interfering structure to an organized wave front pattern. Even within this short distance (2.25 km), temperature profiles exhibited significant spatial variations.

Another type of observations proven useful is surface imaging from ship-based X-band radar. During the experiment, the research vessel (R/V) Oceanus tracked the leading IW front as the IW packet propagated toward the shoreline. In Fig. 1(b), the surface impressions from the radar are overlaid on the top of the thermistor farm location. The benefit of the radar measurement is its coverage, with a diameter of 4–6 km, and also its mobility. In the next section, both ship radar images and thermistor farm measurements will be used for mapping a time-varying, 3D IW temperature field.
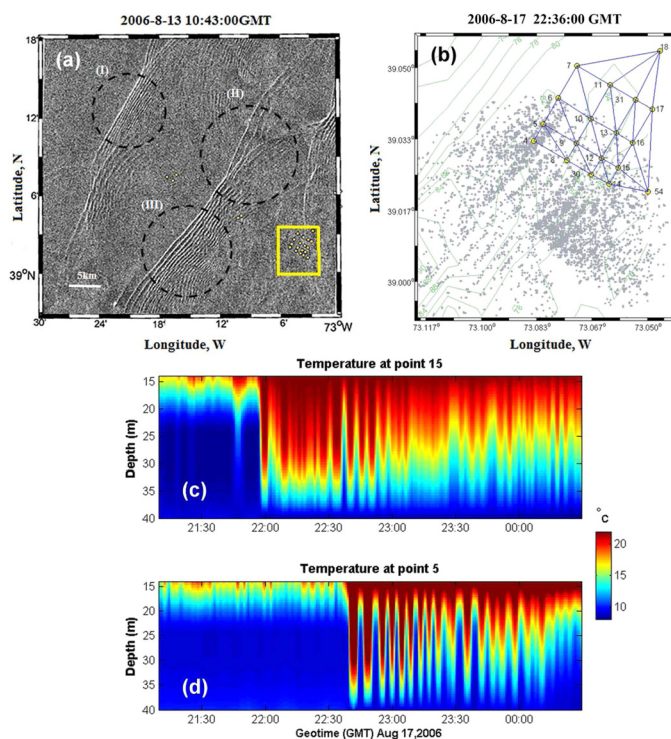
Fig. 1. (Color online) (a) Satellite picture of internal wave packets on 13 August 2006 showing various wave front features. (b) Enlarged map of the yellow box in (a) showing the experimental area with bathymetric contours. The locations of thermistor farm containing 18 vertical arrays and their labels are represented by small circular numbered dots. The footprint of the ship's radar (shown by gray dots) is also shown for the event on 17 August 2006. (c) and (d) Propagation of the internal wave packet through the thermistor farm showing measured temperature profiles at thermistors #15 and #5, respectively.

3. Reconstruction of a 3D internal wave temperature field

The temperature field of a relatively large area, for example, at least many square kilometers, needs to be obtained to study IW impacts on low acoustic frequencies. In this section, we will demonstrate how to reconstruct a 3D IW field using two types of measurements: data from the thermistor farm and surface impressions from ship-based radar. Such a reconstruction is achieved in two steps. First, data interpolation within the thermistor farm is performed. Then the interpolated temperature field is extended with the aid of the radar images. Prior to interpolation, the correlation coefficients in both along-shelf (thermistors #15 and #17) and cross-shelf (thermistors #15 and #5) directions were calculated using the measured temperature data for the first eight IW fronts. The minimum correlation coefficients were greater than 0.70 among the thermistor moorings. This indicates that the correlation of the IW field was high within the thermistor farm that was designed using a logarithmic spacing between moorings in both along-shelf and cross-shelf directions. Therefore, the measurements could be aliased for the later waves in a wave train. The cross-shelf correlation coefficients calculated between thermistors #15 and #17 showed that the later waves were slightly less correlated (0.75 for the first four leading IW fronts and 0.72 for the subsequent four fronts), but the measurements were not aliased from the thermistor farm sampling. To obtain the interpolated field, the thermistor farm area was divided into 24 triangles as shown in Fig. 1(b). Within these small triangular areas, the IW packet was assumed to have constant speed. As shown in Figs. 1(c) and 1(d), the IW fronts at each thermistor string can be identified. The leading wave front with the maximum amplitude was used to calculate

arrival times at all the thermistor string locations. The arrival time and the time-evolving temperature field at any point within each triangle were obtained using a Barycentric interpolation method widely used in computer graphics and geometry processing. The interpolation is shown by Eqs. (1) and (2), respectively,

$$t_0(\alpha, \beta, \gamma) = \alpha t_1 + \beta t_2 + \gamma t_3, \tag{1}$$

$$T_0(\alpha, \beta, \gamma, z, t) = \alpha T_1(z, t + t_1 - t_0) + \beta T_2(z, t + t_2 - t_0) + \gamma T_3(z, t + t_3 - t_0), \tag{2}$$

where $\alpha + \beta + \gamma = 1$; $\alpha, \beta,$ and $\gamma \in [0, 1]$, are Barycentric coordinates converted from Cartesian coordinates;[14] z is the depth; t_0 and T_0 are the arrival time and temperature at any point within the triangle, respectively; t_i and T_i, i = 1, 2, and 3, are the measured arrival times and temperatures at the three vertices of the triangle, respectively; $t_i - t_0$, is the arrival time difference between the point and the vertices. The coordinates ($\alpha, \beta,$ and γ) of any point of the triangle are used as the weighting factors and are proportional to the distance between the point and one of the edges. If one of the coordinates is 0, the corresponding point is on the edge. If two of the coordinates are 0, the corresponding point is one of the vertices. During the experiment, other measurements (e.g., CTD sensors and ship-based ACDPs) indicated a stable isothermal warmer surface layer above 14 m and a stable isothermal cooler bottom layer below 40 m. Here, the Barycentric interpolation was only performed to obtain the temperature field between 14 and 40 m. Figure 2(a) shows the interpolated temperature field at the depth of 28.5 m for 22:36:00 Greenwich Mean Time (GMT) on 17 August 2006, when a strong IW packet propagated through the thermistor farm. Except for the first wave front showing a distinctly stronger feature, the later wave fronts had a complicated spatial structure with different curvatures, interference features, and wave front bifurcation. These were similar to what was observed in satellite images [see Fig. 1(a)]. As shown in Fig. 2(a), the thermistor farm can provide detailed, time-evolving
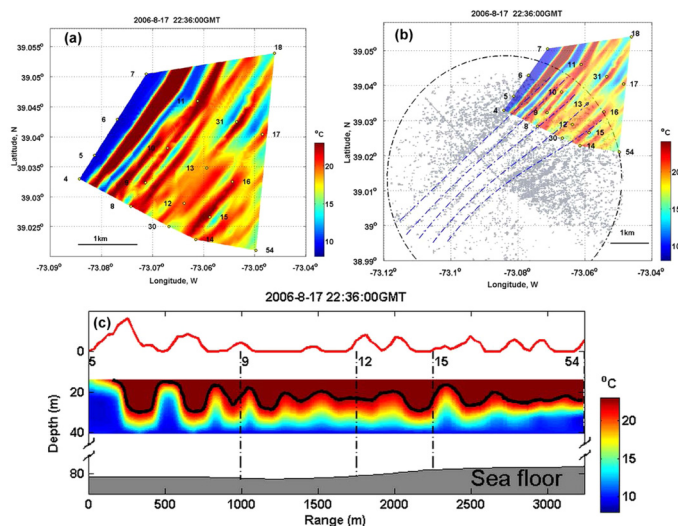
Fig. 2. (Color online) (a) Interpolated temperature data (28.5 m below sea surface) within the thermistor farm at 22:36:00 on 17 August 2006. (b) The ship's radar image (in gray dots) is overlaid by interpolated temperature data. The circle shows the area of radar coverage. The dashed-dotted lines represent the wave fronts obtained by fourth order polynomial fitting of the bright bands on the radar image. The internal wave front patterns shown on the radar image are continuations of the fronts shown from thermistor data. (c) Interpolated temperature profile between 14 and 40 m in the water column as a function of range during its propagation. The solid curve below represents the temperature contour at 22 °C.

temperature profiles over a designated area. This area, even with 18 moorings, was limited for low frequency acoustical modeling. By contrast, a single radar, for example the radar onboard of the R/V Oceanus, can provide a foot-print comparable to that of the thermistor farm. The ship radar image, showing alternating bright and dark bands, is overlaid with the Barycentric interpolated temperature field in Fig. 2(b). As shown in Fig. 1(b) and also Fig. 2(b), five major wave fronts can be seen from the ship radar image. To precisely identify each wave front, a fourth order polynomial fitting of the bright bands with high radar backscatter intensity was performed. The wave fronts obtained from the radar image are shown by dashed lines in Fig. 2(b). Some of the thermistor farm area was covered by the radar foot print. The wave fronts identified by polynomial fitting largely overlapped with the ones seen from temperature data. This suggested the radar images can be used to infer IW wave fronts and their curvature when there are no temperature measurements. However, there are limits to such inferences that depend on the physics of the radar backscatter as well as the subsurface oceanographic conditions. Figure 2(c) shows the side view of the interpolated temperature field along the track connecting the thermistors #54, #15, #12, #9, and #5. The normalized intensity of radar backscatter from the sea surface for this track is also shown by a line on the top. The leading wave front observed in the interpolated temperature field showed strong correlation with strong radar backscattering intensity. Such a statement is also true for the second and third wave fronts. However, the correlation between the temperature field and the radar backscattering intensity was not consistent for later wave fronts. This may be due to noisy radar backscatter signals or due to the complicated IW structure for later wave fronts in the group. This inconsistency is an interesting point for future research, and it is not within the scope of this letter. It is natural to combine the two types of simultaneous measurements (i.e., thermistor data and ship's radar images) to reconstruct the IW field over a larger region. The curvature of the IW fronts from radar images shown as dashed-dotted curves in Fig. 2(b) was used for the extrapolation. Assuming the temperature profiles along the IW fronts under the radar image are the same as the corresponding ones on the edge of the thermistor farm (#54,14,30,8,4), we can extrapolate the temperature field and obtain the reconstructed field shown in Fig. 3(a). For comparison, an alternative extrapolation method is to utilize a non-curved IW front assumption used in some modeling efforts. This resulted in a different temperature field as shown in Fig. 3(b). Acoustic propagation modeling is performed to demonstrate the impact of the two different reconstructed IW fields (i.e., the curved and non-curved wave fronts). It is noted that there are no acoustic data (i.e., both source-receiver) within the footprint of the reconstructed environments. Hence, acoustic modeling is used to make the point here. The reconstructed temperature fields shown in Figs. 3(a) and 3(b) were fed to a 3D parabolic equation as environmental inputs.[15] The 3D parabolic equation uses the split-step Fourier marching algorithm in the Cartesian coordinate. A half-space bottom model with constant seabed sound speed (1650 m/s) and attenuation (0.5 dB/λ) were used in the 3D parabolic equation runs. The source depth was 68.5 m, which was 10 m above the bottom. The source location is shown as a star in Figs. 3(c) and 3(d). The resulting depth-integrated acoustic intensity at 250 Hz is also shown in Figs. 3(c) and 3(d), corresponding to Figs. 3(a) and 3(b). In both cases, the acoustic fields exhibit strong azimuthal and range-dependent fluctuations. It is important to note that the acoustic field shown between Fig. 3(c) and Fig. 3(d) illustrates clear differences over the interpolated area. To quantitatively assess the acoustic difference from the two reconstructed IW fields, the depth-integrated acoustic intensity at a range of 7 km is shown in Fig. 3(e) for both cases. The non-curved case resulted in acoustic fluctuations of up to 7 dB. The curved case resulted in acoustic fluctuations of up to 10 dB. Further, the largest discrepancy between the two cases was more than 7 dB, which amounted to the intensity fluctuation of the non-curved wave front case. These results show that acoustic interactions with IWs were highly sensitive to the curvature of the IWs when the azimuthal angle between the IW fronts and the source-receiver track were small ($\pm 11°$).
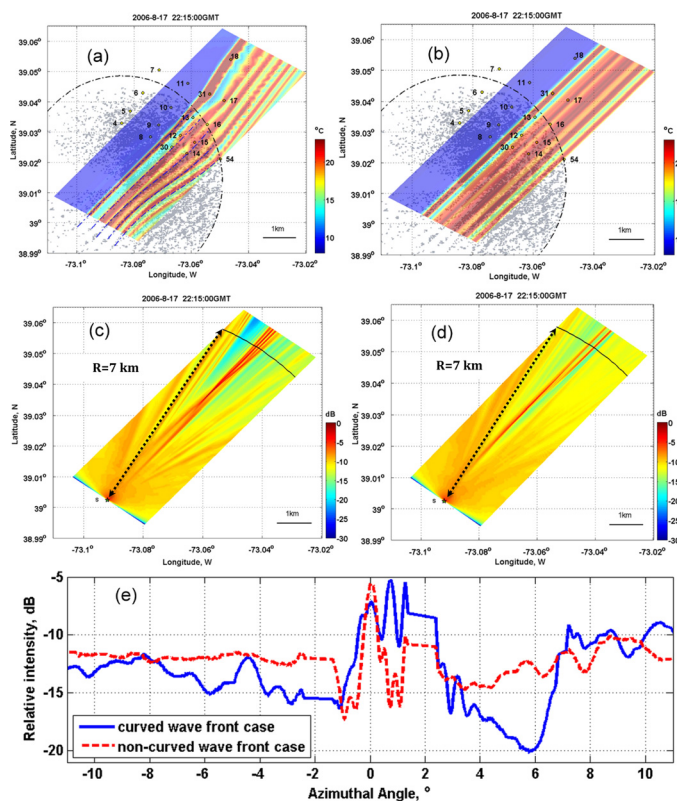
Fig. 3. (Color online) (a) Re-constructed temperature field (28.5 m below sea surface) at 22:15:00 GMT on 17 August 2006 obtained by extrapolating the temperature data within the thermistor farm. The curvature of the internal wave front within the thermistor farm is extended to the larger area under the radar coverage and is considered in the extrapolation. (b) Similar extrapolation using straight line internal wave fronts. (c) Acoustic field calculated using curved internal wave fronts. (d) Acoustic field calculation using straight-line internal wave fronts. (e) Relative acoustic intensity versus azimuthal angle at a range of 7 km. Note the result for the straight-line wave front case [(d)] shows substantial differences at some angles from the more realistic, curved wave front case [(c)]. The azimuthal angle is 0 when the IW front is parallel to the acoustic propagation direction.

4. Discussion and summary

We have presented an observation-based strategy to get the fine structure of time-evolving IW field over a relatively large region (about $8 \, \mathrm{km} \times 8 \, \mathrm{km}$). This strategy mainly utilizes two types of measurements that were collected simultaneously: dense observations from multiple thermistor strings and images from a ship-based X-band radar. The former provides temperature profiles over time when the IWs pass through the mooring region. The latter provides surface expressions of the propagating IWs when the waves travel inshore. Using the unique data from the SW06 experiment, we show that the combined strategy can provide a region of propagating IWs over the continental shelf. The curvature of the IWs and other dynamic features were thus replicated. Due to experimental limitations, there are no source-receiver geometries within the reconstructed footprint of the IW data. Therefore, we use the three-dimensional PE model and reconstructed sound speed input data to show the utility of the proposed method. Three-dimensional acoustic parabolic equation modeling was applied, using the reconstructed environmental data of the IW field. It is shown that the realistic reconstructed environmental data can substantially change a realization of the intensity of the 3D predicted acoustic field when compared with a simple straight line IW model as shown in Fig. 3(e).

It is worthwhile to mention that the detailed measurements from the thermistor farm and the interpolation results are unique by themselves. They can be valuable as ground truth in verifying internal wave modeling efforts. We show that the combined strategy using the thermistor farm and the radar images can provide an extended coverage for mapping internal waves. One variant of this strategy can be combining satellite or ship-based radar images with just one moored thermistor string. This will provide useful inputs to acoustic models at low costs. Also, it is noticed that obtaining this kind of input will be very useful in statistical assessment of important acoustic parameters such as scintillation index (SI) versus range, frequency, and azimuth, which is our future plans.

Acknowledgments

References and links

[1] J. R. Apel, L. A. Ostrovsky, Y. A. Stepanyants, and J. F. Lynch, "Internal solitons in the ocean," Report No. WHOI-2006-04, Woods Hole Oceanographic Institution, Woods Hole, MA, 2006.

[2] J. X. Zhou, X. Z. Zhang, and P. H. Rogers, "Resonant interaction of sound wave with internal solitons in the coastal zone," J. Acoust. Soc. Am. **90**, 2042–2054 (1991).

[3] M. Badiey, Y. Mu, J. F. Lynch, J. R. Apel, and A. N. Wolf, "Temporal and azimuthal dependence of sound propagation in shallow water with internal waves," IEEE J. Ocean. Eng. **27**, 117–129 (2002).

[4] M. Badiey, B. G. Katsnelson, J. F. Lynch, S. Pereselkov, and W. L. Siegmann, "Measurement and modeling of three-dimensional sound intensity variations due to shallow water internal waves," J. Acoust. Soc. Am. **117**, 613–625 (2005).

[5] M. Badiey, B. G. Katsnelson, J. F. Lynch, and S. Pereselkov, "Frequency dependence and intensity fluctuations due to shallow water internal waves," J. Acoust. Soc. Am. **122**, 747–760 (2007).

[6] J. F. Lynch, J. A. Colosi, G. G. Gawarkiewicz, T. F. Duda, A. D. Pierce, M. Badiey, B. G. Katsnelson, J. E. Miller, W. L. Siegmann, C.-S. Chiu, and A. E. Newhall, "Consideration of fine-scale coastal oceanography and 3-D acoustics effects for the ESME sound exposure model," IEEE J. Ocean. Eng. **31**, 33–48 (2006).

[7] M. Badiey, B. G. Katsnelson, Y.-T. Lin, and J. F. Lynch, "Acoustic multipath arrivals in the horizontal plane due to approaching nonlinear internal waves," J. Acoust. Soc. Am. **129**, EL141–EL147 (2011).

[8] K. G. McMahon, L. K. Reilly-Rasaka, W. L. Siegmann, J. F. Lynch, and T. F. Duda, "Horizontal Lloyd mirror patterns from straight and curved internal waves," J. Acoust. Soc. Am. **131**, 1689–1700 (2012).

[9] J. F. Lynch, Y.-T. Lin, T. F. Duda, and A. E. Newhall, "Acoustic ducting, reflection, refraction, and dispersion by curved nonlinear internal waves in shallow water," IEEE J. Ocean. Eng. **35**, 12–27 (2010).

[10] Y.-T. Lin, K. G. McMahon, J. F. Lynch, and W. L. Siegmann, "Horizontal ducting of sound by curved nonlinear internal gravity waves in the continental shelf areas," J. Acoust. Soc. Am. **133**, 37–49 (2013).

[11] W. Alpers, "Theory of radar imaging of internal waves," Nature **314**(6008), 245–247 (1985).

[12] R. Ramos, B. Lund, and H. Graber, "Determination of internal wave properties from X-Band radar observation," IEEE J. Ocean. Eng. **36**, 1039–1047 (2009).

[13] A. Newhall, T. F. Duda, K. von der Heydt, J. Irish, J. Kemp, S. Lerner, S. Libertore, Y.-T. Lin, J. F. Lynch, A. Maffei, A. Morozov, A. Scmelev, C. Sellers, and W. Witzell, "Acoustic and oceanographic observations and configuration information for the WHOI moorings from the SW06 Experiment," Report No. WHOI-2007-04, Woods Hole Oceanographic Institution, Woods Hole, MA, 2007.

[14] P. Shirley and S. Marschner, *Fundamentals of Computer Graphics*, 2nd ed. (A K Peters, Wellesley, MA, 2005), pp. 43–46, 63–67.

[15] T. F. Duda, "Initial results from a Cartesian three-dimensional parabolic equation acoustical propagation code," Report No. WHOI-2006-14, Woods Hole Oceanographic Institution, Woods Hole, MA, 2006.